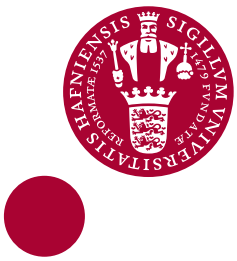

Summer comes to the Southern Ocean

how phytoplankton shape bacterioplankton communities far into the deep dark sea

Richert, Inga; Yager, Patricia L.; Dinasquet, Julie; Logares, Ramiro; Riemann, Lasse; Wendeberg, Annelie; Bertilsson, Stefan; Scofield, Douglas G.

Published in:
Ecosphere (Washington, D.C.)

DOI:
10.1002/ecs2.2641

Publication date:
2019

Document version
Publisher's PDF, also known as Version of record

esa

ECOSPHERE

Summer comes to the Southern Ocean: how phytoplankton shape bacterioplankton communities far into the deep dark sea

INGA RICHERT,[1,2,]† PATRICIA L. YAGER,[3] JULIE DINASQUET,[4,5] RAMIRO LOGARES,[6] LASSE RIEMANN,[4] ANNELIE WENDEBERG,[2] STEFAN BERTILSSON,[1,7] AND DOUGLAS G. SCOFIELD[8,9]

[1]*Department of Ecology and Genetics: Limnology, Uppsala University, Uppsala, Sweden*
[2]*Department of Environmental Microbiology, Helmholtz Centre for Environmental Research – UFZ, Leipzig, Germany*
[3]*Department of Marine Science, University of Georgia, Athens, Georgia, USA*
[4]*Department of Biology, University of Copenhagen, Helsingør, Denmark*
[5]*Scripps Institution of Oceanography, UCSD, San Diego, California, USA*
[6]*Institute of Marine Sciences, CSIC, Barcelona, Spain*
[7]*Science for Life Laboratory, Uppsala University, Uppsala, Sweden*
[8]*Department of Ecology and Genetics: Evolutionary Biology, Uppsala University, Uppsala, Sweden*
[9]*Uppsala Multidisciplinary Center for Advanced Computational Science, Uppsala University, Uppsala, Sweden*

Citation: Richert, I., P. L. Yager, J. Dinasquet, R. Logares, L. Riemann, A. Wendeberg, S. Bertilsson, and D. G. Scofield. 2019. Summer comes to the Southern Ocean: how phytoplankton shape bacterioplankton communities far into the deep dark sea. Ecosphere 10(3):e02641. 10.1002/ecs2.2641

Abstract. During austral spring and summer, the coastal Antarctic experiences a sharp increase in primary production and a steepening of biotic and abiotic gradients that result from increased solar radiation and retreating sea ice. In one of the largest seasonally ice-free regions, the Amundsen Sea Polynya, pelagic samples were collected from 15 sites during a massive *Phaeocystis antarctica* bloom in 2010/2011. Along with a suite of other biotic and abiotic measurements, bacterioplankton were collected and analyzed for community structure by pyrosequencing of the 16S rRNA gene. The aims were to identify patterns in diversity and composition of heterotrophic bacterioplankton and to test mechanistic hypotheses for explaining these differences along variations in depth, water mass, phytoplankton biomass, and organic and inorganic nutrients. The overall goal was to clarify the relationship between primary producers and bacterioplankton community structure in the Southern Ocean. Results suggested that both epipelagic and mesopelagic bacterioplankton communities were structured by phytoplankton blooming in the euphotic zone. As chlorophyll *a* (chl-*a*) increased in surface waters, the abundance of surface bacterioplankton increased, but their diversity decreased. Similarity in bacterioplankton community composition between surface-water sites increased as the bloom progressed, suggesting that algal blooms may homogenize surface-water bacterioplankton communities at larger spatial scales. Below the euphotic zone, the opposite relationship was found. Mesopelagic bacterioplankton diversity increased with increasing chl-*a* in the overlying surface waters. This shift may be promoted by several factors including local increase in organic and inorganic nutrients from particles sinking out of the euphotic zone, an increase in niche differentiation associated with the particle flux, interactions with deep-dwelling macrozooplankton, and release from competition with primary producers. Additional multivariate analyses of bacterioplankton community structure and nutrient concentrations revealed distinct depth horizons, with bacterioplankton communities having maximum alpha and beta diversity just below the euphotic zone, while nutrient composition gradually homogenized with increasing depth. Our results provide evidence for bloom-driven (bottom-up) control of bacterioplankton community diversity in the coastal Southern Ocean and suggest mechanisms whereby surface processes can shape the diversity of bacterioplankton communities at great depth.

Key words: Amundsen Sea Polynya; Antarctica; bacterioplankton diversity; chlorophyll *a; Phaeocystis antarctica;* phytoplankton bloom; Southern Ocean.

Received 22 December 2018; accepted 11 January 2019. Corresponding Editor: Sean Powers.

† **E-mail:** inga.richert@gmail.com

Introduction

In seasonally ice-free waters of the Southern Ocean, such as the Amundsen Sea Polynya (ASP), seasonal blooms of phytoplankton provide the main source of organic matter. Fixation and export of atmospheric carbon into the ocean interior occur via vertical mixing, partial decomposition, and eventual sinking of photosynthetically produced organic material. Polar oceans host an active (Ducklow and Yager 2007, Williams et al. 2016) and diverse (Yager et al. 2001, Ghiglione et al. 2012, Delmont et al. 2014, Kim et al. 2014, Richert et al. 2015) bacterioplankton community. At any given location and time in the environmentally patchy ASP (Yager et al. 2012, Mu et al. 2014), several factors could play a role in shaping the bacterioplankton community, including interactions with the phycosphere (Delmont et al. 2014, 2015, Seymour et al. 2017), niche differentiation associated with the particle flux or marine snow (Azam 1998, Kiørboe and Jackson 2001, Azam and Malfatti 2007), and the bioavailability of particulate organic carbon (Ducklow et al. 2015, Williams et al. 2016) and dissolved organic compounds (Sipler and Connelly 2015, Dinasquet et al. 2017), which represent potential substrates for heterotrophic bacteria. Other factors may include irradiance (Bryant and Frigaard 2006, Gómez-Consarnau et al. 2007) as well as interactions across trophic levels, in particular the local extent of primary productivity (Arrigo and van Dijken 2003, Alderkamp et al. 2012, 2015, Schofield et al. 2015) and macrozooplankton (Wilson et al. 2015). Additionally, physical gradients that shape hydrography and separate water masses based on temperature–salinity signatures can also control the distribution of microbial communities (Galand et al. 2010, Agogué et al. 2011, Alonso-Sáez et al. 2011, Ghiglione et al. 2012, Hamdan et al. 2013). Three major water masses were present in the ASP at the time of sampling (Yager et al. 2012, 2016): Antarctic Surface Water (AASW), Winter Water (WW), and modified Circumpolar Deep Water (mCDW; Randall-Goodwin et al. 2015).

The composition of the bacterioplankton community within the ASP varies with depth (Delmont et al. 2014, 2015, Kim et al. 2014, Richert et al. 2015). A major portion of the bacterioplankton community in the seasonal surface waters of the ASP are light-adapted, fast-growing copiotrophs, including members of the *Flavobacteria*, *Polaribacter*, *Gammaproteobacteria* SAR92, and *Oceanospirillaceae*. The bacterioplankton communities within deeper mesopelagic waters are comprised of a more diverse heterotrophic community including numerous representatives of, for example, the classes Flavobacteriia, Alphaproteobacteria, and Gammaproteobacteria (Delmont et al. 2014, 2015, Kim et al. 2014, Richert et al. 2015). Metagenome data demonstrate that an oligotrophic life strategy is dominant in the ocean's free-living microbial populations (Lauro et al. 2009).

At the time of sampling (13 December 2010–15 January 2011), the polynya was characterized by the initiation and buildup of a massive phytoplankton bloom consisting mostly of the colonial microeukaryote *Phaeocystis antarctica* (Yager et al. 2016), and the downward particle flux was mainly phytodetrital aggregates (Ducklow et al. 2015), consistent with the relatively low numbers and subsurface maxima of macrozooplankton observed during ASPIRE (Wilson et al. 2015). The general goal was to identify how the local environment, in particular the local phytoplankton biomass, acted upon the composition and diversity of heterotrophic bacterioplankton communities during the ephemeral phytoplankton bloom characteristic of the coastal Antarctic.

The first question was how the algal bloom would affect bacterial community diversity at the surface. In their review, Horner-Devine et al. (2004) cite multiple lines of evidence for how bacterial diversity varies with primary productivity in ways similar to plants and animals, with high productivity increasing homogeneity and reducing diversity, especially for some taxonomic groups. In the ASP, bacterial biomass and activity increases with phytoplankton biomass (Williams et al. 2016), but bacterial carbon adds up to

only about 1–2% of algal carbon, with microzooplankton and zooplankton biomass adding up to about 5% (Yager et al. 2016). Thus, the massive bloom of a near-monoculture of *Phaeocystis antarctica* dominates the available substrate for bacteria. Such substrate homogeneity might reduce bacterial diversity. Competition with phytoplankton for nutrients (iron in particular) might also limit heterotrophic bacterial diversity —but not abundance—by favoring a bacterioplankton community composed primarily of opportunistic or mutualistic taxa with high-affinity siderophores (Reid et al. 1993, Barbeau et al. 2001). Alternatively, epipelagic bacterioplankton communities could simply represent stochastic subsets of existing communities, in which case no relationship would be observed between bacterial community diversity and phytoplankton productivity.

The second question was about the fate of the bloom and its potential impact on the mesopelagic bacterial community structure. The sedimenting flux of detritus is known to be an important factor structuring bacterioplanktonic communities below the euphotic zone (Pelve et al. 2017), and most of the ocean's surface-generated organic matter undergoes recycling in the mesopelagic ocean (Buesseler et al. 2007, Buesseler and Boyd 2009, Giering et al. 2014). Carbon budgets suggest, and measurements confirm, that significant mesopelagic bacterial activity occurs in the ASP (Ducklow et al. 2015, Williams et al. 2016, Yager et al. 2016) below the bloom. Here, we asked whether the deep bacterial community in the ASP shift in response to the sinking bloom, or if it was it poised from the start and steady throughout the season. A related question was whether or not the arrival of the sinking particles increases diversity.

To address these questions, physical characteristics and planktonic communities were sampled at five depth horizons that covered stations along the entire ASP and its edges during the austral summer of 2010–2011. Stations covered the full range of bloom stages (pre-bloom in the pack ice to high bloom in the central open polynya; Yager et al. 2016). Correlation and regression modeling and multivariate statistical analyses were applied to explore linkages between environmental gradients and bacterial abundance and diversity. Our results suggest that the phytoplankton bloom clearly impacts bacterioplankton community composition across the surface waters of the polynya and deep into the mesopelagic.

Methods

Sampling

Sampling was conducted during the Amundsen Sea Polynya International Research Expedition (ASPIRE) in the late spring and early austral summer (November 2010–January 2011) when the research icebreaker RVIB *Nathaniel B. Palmer* cruised the Amundsen Sea Polynya (71–75°S, 110–120°W) and its marginal zones (Yager et al. 2012, 2016). To the south, the polynya meets the Antarctic continent, surrounded by ice shelves (such as the Dotson Ice Shelf and Getz Ice Shelf) and the Antarctic land mass. The northern border represents the marginal ice zone and pack ice between the polynya and the open ocean. Sampling sites covered all parts of the polynya, including sites close to the continent and ice shelves, within the open polynya, close to the marginal ice zones and underneath the pack ice. Altogether, vertical sample profiles were collected from 15 stations (Fig. 1).

At each station, probes coupled to an array of remotely controlled sampling bottles were used for parameter acquisition and sampling. This CTD (conductivity–temperature depth probe) rosette included sensors reading depth-resolved profiles of temperature (°C), conductivity (S/m), oxygen (mg/L), chlorophyll *a* (chl-*a*) concentration (mg/m^3, via chl-*a* fluorescence), and photosynthetically active radiation (%PAR) for each cast (SBE 911; Sea-Bird Electronics, Bellevue, Washington, USA). Sensor profiles were monitored during the lowering of the CTD through the water column. Based on these profiles, five depths were chosen for seawater sampling during ascent of the CTD. Typically, the five depths chosen corresponded to (1) near surface (Horizon 1: $H1_{surf}$); (2) chl-*a* fluorescence maximum (Horizon 2: $H2_{cmax}$); (3) base of the high-chlorophyll layer, corresponding to the depth at which the fluorescence drops to a negligible level (Horizon 3: $H3_{csub}$); (4) mesopelagic temperature minimum above the halocline (Horizon 4: $H4_{Tmin}$); (5) near-bottom temperature maximum below the halocline (Horizon 5: $H5_{Tmax}$); and (6) bottom water (Horizon 6: $H6_{bot}$, collected at a subset of

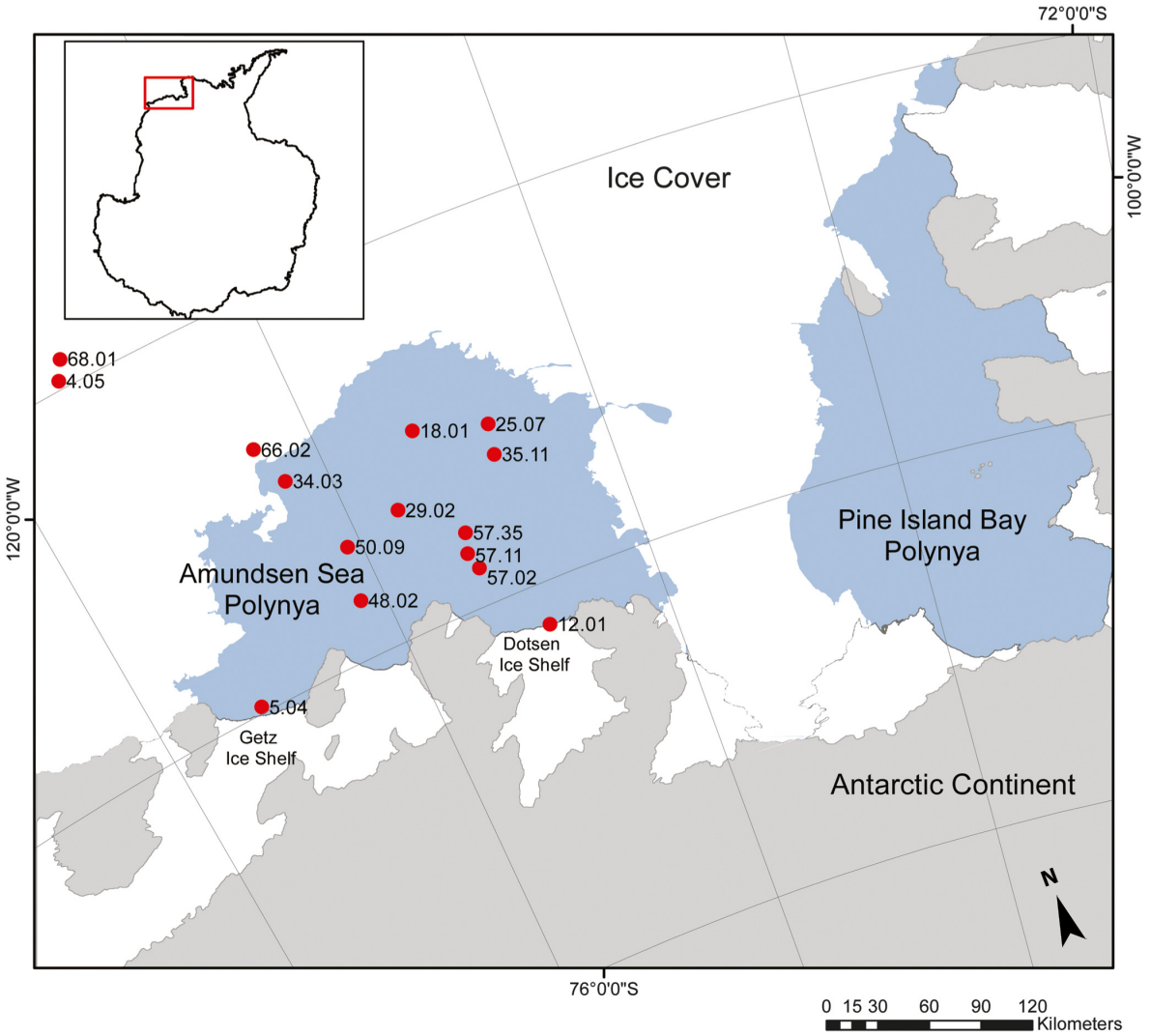

Fig. 1. Sampling locations (labeled with event number; see Table 1; Appendix S2: Table S1 for further details) within and around the Amundsen Sea Polynya, with its ice margins at the time of sampling. Background image from National Snow and Ice Data Center (NSIDC; Haran et al. 2005).

stations). At each depth, seawater was collected in 12-L Niskin bottles attached to a 24-bottle rosette (SBE 32; Sea-Bird Electronics).

Grouping of biotic samples along the depth gradient was done following standard procedures in two alternate and non-exclusive ways, depending on the analysis: (i) by water mass into Antarctic Surface Water (AASW), Winter Water (WW), or modified Circumpolar Deep Water (mCDW) based on their temperature–salinity signature (following Randall-Goodwin et al. 2015) and a fourth category Mix for samples that had temperature/salinity values intermediate between WW and mCDW; or ii) by the fixed factor depth horizons at which the samples were taken (as described in this section): (1) $H1_{surf}$, (2) $H2_{cmax}$, (3) $H3_{csub}$, (4) $H4_{Tmin}$ (deep Winter Water), (5) $H5_{Tmax}$ (upper mCDW), and (6) $H6_{bot}$ (lower mCDW). Note that grouping (ii) represents a more highly resolved classification, with Horizons 1–3 in the euphotic region and Horizons 4–6 in the mesophotic region, and that grouping (i) and some divisions between horizons in grouping (ii) are dependent upon

halocline and thermocline boundaries and thus have variable depths among sampling stations. The extent to which these classification schemes differ in explanatory power for determining the diversity and structure of heterotrophic bacterioplankton communities is discussed below.

Bacterial community analysis

DNA was extracted from 0.2-μm filtered seawater samples using a phenol–chloroform extraction (Riemann et al. 2000). Prior to extraction, microbial cells were enzymatically digested for 30 min with lysozyme at 37°C followed by an overnight digestion with Proteinase K (both 20 mg/mL; Sigma-Aldrich, Darmstadt, Germany) at 55°C (Boström et al. 2004). The 16S rRNA genes were amplified using the bacterial primers Bakt_341F (CCTACGGGNGGCWGCAG) and Bakt_805R (GACTACHVGGGTATCTAATCC) with 454-Lib-L adapters and sample-specific barcodes on the reverse primer (Herlemann et al. 2011). Barcodes for specific samples are found in Appendix S2: Table S1. Triplicate 20-μL PCRs for each sample were carried out with 10–70 ng extracted environmental DNA as template, and Phusion Hot Start High-Fidelity DNA Polymerase (Thermo Scientific, Göteborg, Sweden) at the thermal conditions: initial denaturation at 98°C for 30 s, followed by 25 cycles of an initial 98°C denaturation for 30 s, subsequent annealing at 50°C for 30 s, and 30-s extension at 72°C. These 25 cycles were followed by a final 7-min extension at 72°C. Triplicate reactions were pooled, purified (Agencourt AMPure XP Kit; Beckman Coulter, Bromma, Sweden), and quantified (PicoGreen; Invitrogen, Stockholm, Sweden). Equimolar amounts of amplicons from each sample were pooled and sequenced by 454 pyrosequencing using Titanium chemistry at the SNP&SEQ SciLifeLab platform hosted by Uppsala University (Sweden).

In order to obtain a list of observed operational taxonomic units (OTUs) suitable for statistical analyses, low-quality sequences were removed from the dataset, and sequencing noise was reduced using AmpliconNoise v1.24 (Quince et al. 2011) with default parameters. AmpliconNoise implements algorithms that remove PCR and 454-pyrosequencing errors, as well as the tool Perseus, which removes chimeric sequences. Reads that did not carry the exact primer sequence were also removed. The raw sequence data are archived at the European Nucleotide Archive (ENA) under accession no. PRJEB4866. With a length cutoff of 425 base pairs (bp), the remaining reads were processed using the Quantitative Insights Into Microbial Ecology (QIIME) software v1.3 (Caporaso et al. 2010). Sequences were clustered into OTUs at 97% pairwise identity using UCLUST (Edgar 2010). Taxonomic assignments of representative sequences from each OTU were obtained according to the SILVA111 database (Quast et al. 2013) by using the RDP classifier implemented in QIIME (Wang et al. 2007). OTUs that were assigned to the same taxa were not merged. After clustering and taxonomy assignment, the raw data table contained 214,949 reads. Singleton sequences were removed (7894 reads), as well as reads from OTUs that could not be classified (2094 reads), and eukaryotic chloroplasts, which were identified as *Cyanobacteria* (25,025 reads) and *Archaea* (1748 reads). The remaining 178,188 reads were used for further analyses.

Bacterial abundance

Samples (1.5 mL) for bacterial enumeration were fixed with EM-grade glutaraldehyde (1% final conc.; Sigma, Darmstadt, Germany), flash-frozen in liquid N_2, and stored at −80°C. Bacteria were enumerated in a FACSCanto II flow cytometer (Becton Dickinson, Franklin Lakes, New Jersey, USA) after staining the fixed cells with SYBR Green (Invitrogen, Tåstrup, Denmark; Gasol and del Giorgio 2000). The sample volume was calibrated with fluorescent beads.

Nutrient and organic matter data

Water samples were collected, pre-filtered (0.45 μm), and analyzed for nitrite, nitrate, ammonia, silicate, and orthophosphate using an autoanalyzer onboard the ship (for details, see Yager et al. 2016). All samples for dissolved organic carbon (DOC), total nitrogen (TN), particulate organic carbon (POC), and particulate organic nitrogen (PON) analysis were collected, and analyzed using standard protocols (for details, see Yager et al. 2016).

Chlorophyll a fluorescence: a proxy for phytoplankton biomass and bloom stage

Phytoplankton biomass was estimated by Chlorophyll *a* (chl-*a*) fluorescence in several

different ways. Discrete samples were collected using Niskin bottles. Some were analyzed shipboard with a fluorometer calibrated with spinach standards; others were analyzed using HPLC (Alderkamp et al. 2015, Yager et al. 2016). Continuous chl-*a* profiles were also obtained at each station using calibrated in vivo chl-*a* fluorescence traces from the CTD probe. When using chl-*a* as a proxy for phytoplankton, it was recognized that photopigment content additionally depends on taxonomy and physiological state of the phytoplankton (Longhurst and Glen Harrison 1989). Particulate organic carbon (POC) was collected from the water column at the same depths as chl-*a*. Concentrations of chl-*a* correlated positively with POC concentrations (Yager et al. 2016), with the POC:chl-*a* ratio in the upper water column ranging from 37 to 115 (median = 44).

For each station, the primary measure of the bloom extent was the maximum chl-*a* concentration observed at each station, chl-*a* max. A second measure was also used: integrated chl-*a*, calculated via numerical integration of chl-*a* concentration profiles (for further methodological details, see Appendix S1). Integrated chl-*a* represents chl-*a* concentration throughout the depth profile of each station and was positively correlated with chl-*a* max (Pearson's $\rho = 0.802$, $P < 0.001$; Appendix S1: Fig. S2). The main text presents correlations vs. chl-*a* max; there are corresponding regression results vs. both chl-*a* max and integrated chl-*a* provided in Appendix S2.

During analysis, unusually noisy chl-*a* traces were observed for Station 5 (Event 5.04; Appendix S1: Fig. S1) that might have been due to fouling of the CTD sensor. Thus, Station 5 was excluded from all regressions involving estimates of integrated chl-*a*. For further details, see Appendix S1.

Diversity calculations

Operational taxonomic units richness of samples was estimated throughout the water column using rarefaction estimates calculated with estimated_observation_richness.py in QIIME 1.9.1 (Caporaso et al. 2010, Colwell et al. 2012). The mean number of reads per sample was 2481 ± 966 (SD) reads (range 751–5600 reads), so richness results are presented using rarefaction with sample size N = 750. Rarefaction curves for a range of sample sizes are presented in Appendix S2: Fig. S1. See Appendix S1 for further methodological details.

Diversity measures were compared and contrasted along environmental gradients using correlation and regression analyses; Pearson correlation coefficients (ρ) are presented in the main text and provide corresponding regression results including slope estimates in Appendix S2. *Alpha diversity* was quantified using both Shannon's H (Shannon 1948) and Simpson's D (Simpson 1949) measures to show that the results are qualitatively robust to our choice of alpha diversity metric. Results in the main text use Shannon's H, and corresponding results using Simpson's D are in Appendix S2. Patterns of bacterioplankton community turnover were examined using delta divergence, which expresses the divergence in diversity between pairs of samples (Scofield et al. 2012).

Beta diversity was estimated using multivariate ordination methods applied to pairwise Bray-Curtis dissimilarity, which account for both presence/absence of OTUs and shifts in their relative abundances (Bray and Curtis 1957), and contrast this with pairwise Euclidean dissimilarity in nutrient levels between samples (Ramette 2007, Legendre and Birks 2012) to examine the extent to which nutrient availability may structure heterotrophic bacterioplankton community diversity. Multivariate homogeneity of group dispersion was also compared to environmental factors that separate the groups (Anderson et al. 2006).

Statistical analysis

All statistical data analyses were done in RStudio using R version 3.3.2. A custom script was used (available at https://github.com/douglasgscofield/pubs/tree/master/Richert-et-al-1) together with scripts for ecological diversity analysis available at https://github.com/douglasgscofield/dispersalDiversity (Scofield et al. 2012) to calculate most diversity statistics directly from the OTU table. Bacterioplankton richness and abundance was compared between depth horizons using ANOVA (function aov), and depth horizon means were compared using Tukey post hoc tests (function TukeyHSD). Samples from the deepest depth horizon $H6_{bot}$ (lower mCDW) were collected from just two stations; for these comparisons, these samples were lumped with those from the $H5_{Tmax}$ (upper mCDW) depth horizon. For comparisons along environmental gradients, Pearson correlation coefficients (function cor.test) and linear regressions (function lm) were calculated.

For multivariate statistical analysis, the vegan package version 2.4-2 in R was used (Oksanen et al. 2013). The number of reads per taxon was standardized by dividing by the total number of reads per sample. The nutrient data and other environmental parameters were transformed linearly to range between 0 and 1 corresponding to the minimum and maximum values across all collected samples (function decostand, method range). Pairwise dissimilarity matrices were calculated among samples for OTUs (N = 72 samples) using Bray-Curtis dissimilarity with presence–absence standardization (function vegdist). The two OTU samples from $H6_{bot}$ were included within the overlying $H5_{Tmax}$ depth horizon for these analyses. Pairwise dissimilarity matrices were calculated among the subset of samples having full seawater nutrient content available (N = 43 samples) using Euclidean distance (function vegdist). None of these samples were assigned to the $H6_{bot}$ depth horizon. Pairwise dissimilarities were used to calculate group dispersions for OTUs and nutrients within each of the five upper depth horizons ($H1_{surf}$ – $H5_{Tmax}$) via PCoA and calculation of group-specific centroids and sample-specific distances from the centroid, as implemented in the function betadisper following the method of Anderson (2006). In brief, the centroid of a group is its spatial median, the point that minimizes the sum of distances to all sample-specific points belonging to that group. The dispersion of samples within each group is the distribution of distances of samples from the centroid so calculated. Tests for homogeneity of dispersions were performed with Tukey post hoc tests as implemented in function TukeyHSD.betadisper. Our interest was primarily in analyzing homogeneity of depth horizon-specific dispersions; apart from qualitative comparisons, we do not include analysis of the group-specific centroids per se. For the 43 samples having both OTU and complete nutrient content data, a non-metric multidimensional scaling (NMDS, function metaMDS) was performed with dissimilarity matrices calculated for OTUs and nutrients as described in this section. The NMDS plot for OTUs was annotated using environmental vectors for nutrients and for phytoplankton biomass, bacterial abundance, and depth, and the NMDS plot for nutrients using environmental vectors for phytoplankton biomass, bacterial abundance, and depth (all annotations with environmental vectors used function envfit). The dissimilarity matrices for OTUs and nutrient content were compared among these samples using a Mantel test (function mantel, Spearman rank correlation) with *P* value calculated via 999 row/column permutations as implemented in the function.

Results

Inventories

From the 15 stations that spanned the entire region (Fig. 1, Table 1) and represented early, mid-, and high-bloom stages (Yager et al. 2016), a total of 72 water samples covered large environmental ranges in temperature (−1.8 to + 1.3°C), salinity (33.4–34.7), bacterial abundance (0.5–8 × 10^8 cells/L), and dissolved organic carbon (0.59–1.44 ppm; Appendix S2: Tables S1, S5). Other measured nutrients (Appendix S2: Table S5) included silicate (SiO_4^{4-}; 66.8–115 μmol/L); total nitrogen (TN; 0.17–0.52 ppm); nitrate (NO_3^-; 9.3–34.2 μmol/L); nitrite (NO_2^-; 0–0.06); and orthophosphate (PO_4^{3-}; 0.76–2.2 μmol/L). The station depth ranged from 400 to 1250 m (Table 1). Chl-*a* varied with depth and across the euphotic zone of the ASP with peak bloom intensity near the surface in the central polynya (Appendix S1: Fig. S1). The maximum concentration of chl-*a* for each station (chl-*a* max) ranged from 0 to 27 mg/m^3, correlated with integrated chlorophyll *a* at each station (Pearson's $\rho = 0.802$, $P < 0.001$; Appendix S1: Fig. S2), and corresponded well with bloom stage (Yager et al. 2016).

Bacterioplankton abundance decreased with depth (Fig. 2b–d; ANOVA among depth horizons, $F_{4,66} = 15.11$, $P < 0.001$), but was similar among the upper three depth horizons (Tukey post hoc tests; $H1_{surf}$ vs. $H2_{cmax}$ $P = 0.99$, $H2_{cmax}$ vs. $H3_{csub}$ $P = 0.30$, $H1_{surf}$ vs. $H3_{csub}$ $P = 0.095$) and between the deep Winter Water and combined mCDW depth horizons (Tukey post hoc test, $H4_{Tmin}$ vs. $H5_{Tmax}$ + $H6_{bot}$, $P = 0.99$).

Bacterioplankton community richness and abundance throughout the water column

Bacterioplankton community richness varied among stations (Fig. 2a), with the highest cumulative richness at Station 4 (late spring in the pack

Table 1. Station parameters for ASPIRE as mapped in Fig. 1.

Station† (event)	Latitude	Longitude	Seafloor depth (m)	Position in polynya	Bloom stage‡	No. sample depth horizons
4.05	71°95′29″S	118°47′26″W	600	Shelf break pack ice	Early bloom	5
5.04	73°96′66″S	118°03′48″W	1250	Getz Ice Shelf	Early bloom	5
12.01	74°20′98″S	112°37′31″W	700	Dotson Ice Shelf	Early bloom	6
18.01	73°00′00″S	113°30′23″W	435	Marginal ice	Mid-bloom	4
25.07	73°12′01″S	112°00′07″W	406	Marginal ice	Mid-bloom	5
29.02	73°35′04″S	114°12′68″W	738	Open polynya	High bloom	5
34.03	72°96′35″S	115°75′96″W	684	Marginal ice	Early bloom	5
35.11	73°27′95″S	112°10′41″W	420	Marginal ice	High bloom	5
48.02	73°70′13″S	115°44′99″W	997	Open polynya	High bloom	5
50.09	73°41′61″S	115°25′03″W	1050	Open polynya	High bloom	5
57.02	73°80′17″S	113°16′5″W	745	Open polynya	High bloom	5
57.11	73°70′73″S	113°26′53″W	745	Open polynya	High bloom	5
57.35	73°60′22″S	113°14′88″W	745	Open polynya	High bloom	5
66.02	72°74′09″S	116°01′99″W	659	Marginal pack ice	Early bloom	4
68.01	71°85′68″S	118°27′98″W	830	Shelf break pack ice	Early bloom	3

† An expanded table containing further details is provided as Appendix S2: Table S1.
‡ Yager et al. (2016).

ice near the shelf break) and the lowest at Stations 66 and 68 (also in the pack ice, but later in the season). Richness increased with depth (Fig. 2b–c; ANOVA among depth horizons, $F_{4,67} = 38.45$, $P < 0.001$). It was similar between $H1_{surf}$ and $H2_{cmax}$ in the photic zone (Tukey post hoc test, $P \approx 1$) and also similar between mesopelagic horizons $H4_{Tmin}$ and $H5_{Tmax}$ + $H6_{bot}$ (Tukey post hoc test, $P \approx 1$). Bacterioplankton richness at $H3_{csub}$ differed from and was intermediate to those in the overlying $H2_{cmax}$ and the underlying $H4_{Tmin}$ (Tukey post hoc tests; $P < 0.001$ and $P < 0.01$, respectively). Rarefaction curves showed that the increase in bacterioplankton community richness with depth was robust to the selection of rarefaction sample number (Appendix S2: Fig. S1).

Surface bacterioplankton communities changed with the bloom progression

Among samples from AASW, there was a negative correlation between the magnitude of a station's chl-*a-max* (bloom stage) and bacterioplankton *alpha diversity* measured by Shannon's H (Fig. 3a; Pearson's $\rho = -0.631$, $t_{21} = -3.725$, $P < 0.01$). There were similar negative correlations between the magnitude of the chl-*a* max and Simpson's *D* (Pearson's $\rho = -0.603$, $t_{21} = -3.462$, $P = 0.002$) and bacterioplankton *richness* (Pearson's $\rho = -0.722$, $t_{21} = -4.784$, $P < 0.001$). This decrease in *alpha diversity* with increasing bloom extent (chl-*a* max) occurred despite a strong positive correlation between bacterioplankton abundance and the chl-*a* max at each station (Fig. 3b; Pearson's $\rho = 0.803$, $t_{21} = 6.169$, $P < 0.001$).

Bacterial community *delta divergence* among AASW samples also decreased as the pairwise mean chl-*a* max of the stations increased (Fig. 4a; Pearson's $\rho = -0.292$, $t_{251} = -4.831$, $P < 0.001$). The correlation was stronger when examined just among pairs of samples from $H2_{cmax}$ (Fig. 4b; Pearson's $\rho = -0.445$, $t_{64} = -3.974$, $P < 0.001$).

Bacterioplankton communities below surface waters also respond to bloom progression

Similar to above, a negative correlation was observed between alpha diversity and bloom extent among samples from $H2_{cmax}$ (Fig. 5a; Pearson's $\rho = -0.628$, $t_{13} = -2.910$, $P = 0.012$). Surprisingly, this relationship reversed to a positive correlation for the horizon $H3_{csub}$ below the euphotic zone (Fig. 5b; Pearson's $\rho = 0.532$, $t_{12} = 2.177$, $P = 0.050$). The correlation remained positive, although not statistically significant, for $H4_{Tmin}$ (deep WW; Fig. 5c; Pearson's $\rho = 0.364$, $t_{12} = 1.360$, $P = 0.200$) and $H5_{Tmax}$ (upper mCDW; Fig. 5d; Pearson's $\rho = 0.364$, $t_{13} = -0.491$, $P = 0.632$). Correlations using integrated chl-*a* as an alternative measure of bloom extent were considerably weaker below $H2_{cmax}$ while remaining qualitatively similar (Appendix S2: Table S3).

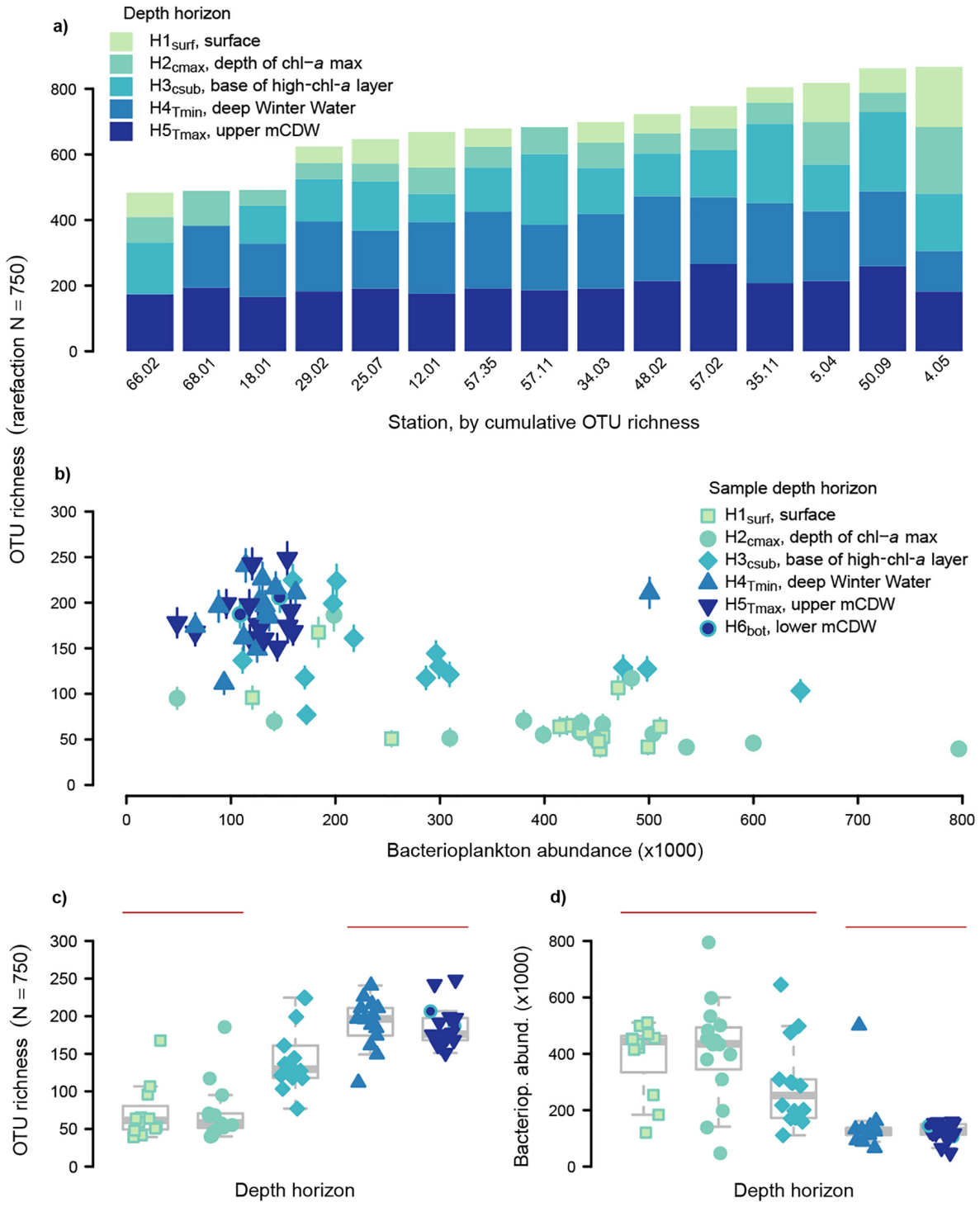

Fig. 2. Bacterioplankton community richness and abundance, by depth horizon and station. Richness was estimated from OTUs and standardized via rarefaction using sample number $N = 750$. (a) Cumulative bacterioplankton richness at each station. The lower mCDW depth horizon (collected from just two stations) is excluded from this panel. (b) Bacterioplankton richness vs. abundance in each sample, with colored symbols indicating

(Fig. 2. *Continued*)
depth horizon. Richness estimates include 95% confidence intervals calculated during rarefaction; see text for further details. (c) Bacterioplankton richness vs. depth horizon. (d) Bacterioplankton abundance vs. depth horizon. Depth horizons in panels (c) and (d) follow the legend in panel (b). Gray box plots show central tendency and quartiles. In panels (c) and (d), the horizontal lines connect depth horizons that did not differ in bacterioplankton richness or abundance, respectively, as determined via pairwise Tukey post hoc tests ($P \leq 0.05$); see text for further details.

As with surface waters, bacterial abundance in $H2_{cmax}$ increased with bloom stage (Appendix S2: Fig. S2a). Deeper in the water column, abundance also increased with bloom stage, although the relationship was statistically significant only at $H5_{Tmax}$ (Appendix S2: Fig. S2a, Table S3).

Beta diversity of bacterioplankton to corresponding nutrient distribution

In our multivariate analyses, OTU samples clustered most strongly according to depth (PCoA1 and NMDS; Fig. 6a, c) with a clear separation between the deep horizons $H5_{Tmax}$ and $H6_{bot}$ from upper horizons $H1_{surf}$ to $H3_{csub}$. Distinct clusters appeared between $H1_{surf}$ and $H2_{cmax}$ clustering together and a separated $H3_{csub,}$ which correspond to the switch in response of bacterioplankton community alpha diversity to chl-*a* shown in Fig. 5. Some outlier samples were collected at stations with reduced influence from the phytoplankton bloom, either at the Dotson Ice Shelf front (station 12.01) or beneath the pack ice (station 68.01).

Nutrients clustered as expected according to depth horizon (see also Yager et al. 2016). Samples from the three upper horizons exhibited greater variability but generally lower inorganic nutrients and higher organic compounds. Samples from the two bottom horizons showed less variability but higher inorganic and lower organic nutrient concentrations. $H3_{csub}$ and $H4_{Tmin}$, which both belong to the Winter Water mass, could be separated by nutrients. The $H3_{csub}$ was characterized by the highest concentration of dissolved organic carbon [DOC] and ammonia [NH_4^+], with DOC in a range from 0.59 to 1.43 ppm and NH_4^+ in a range from 0 to 1.26 μmol/L (Fig. 6c, Appendix S2: Table S5).

Both OTU diversity and nutrients displayed distinct spatial gradients among samples. Both

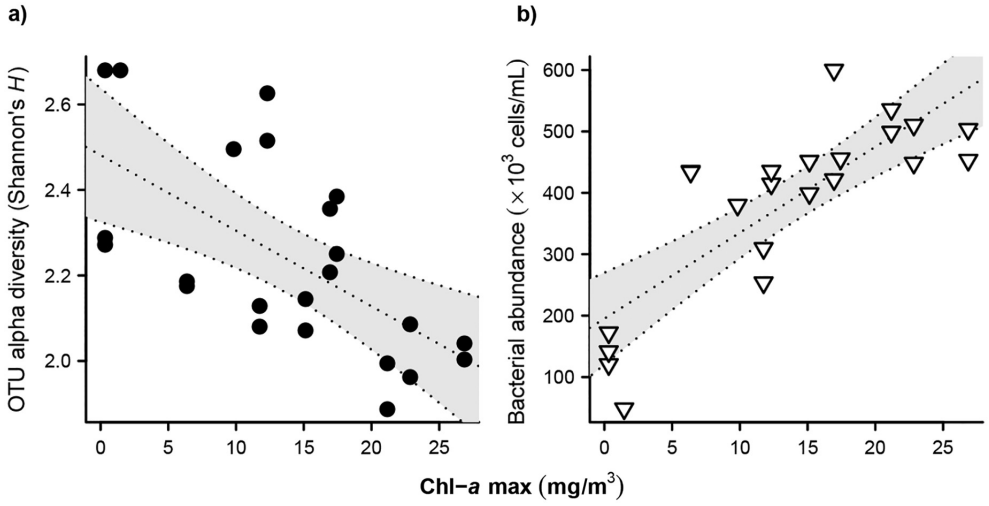

Fig. 3. Linear regression between total surface-water (AASW) diversity measures and bloom progression as measured by the magnitude of the chl-*a* max concentration. (a) Alpha diversity of OTUs found in AASW, as measured by Shannon's *H*; (b) bacterial abundance in AASW. Dotted lines represent linear regression results with shaded 95% confidence range.

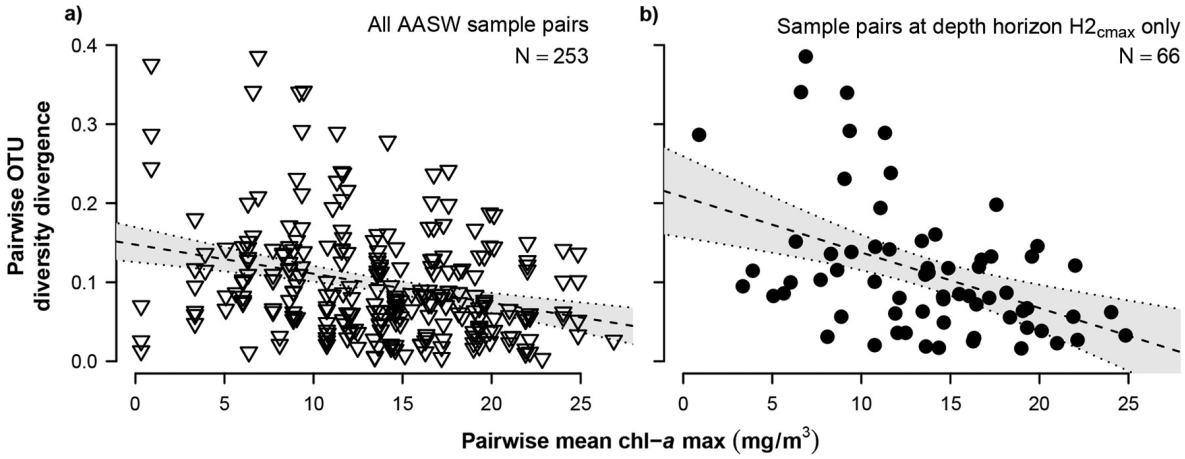

Fig. 4. Linear regression between pairwise divergence and bloom progression as measured by pairwise mean station chl-*a* max. (a) Pairwise comparison of all surface-water samples; (b) pairwise comparison only of samples taken at $H2_{cmax}$, the depth of maximum chl-*a* at each station. Dashed lines represent linear regression results with shaded 95% confidence range.

types of samples separated broadly by depth as shown by the first axes of both OTU diversity and nutrient content in both the beta dispersal and NMDS analyses (Fig. 6a, c, d, f). A positive correlation was observed between Bray-Curtis pairwise distance matrices of sample OTU diversity and sample nutrient content (Mantel test, $r = 0.54$, $P = 0.001$).

Variation in nutrient content among samples, however, showed a more linear (or monotonic) relationship with depth than did variation in OTU diversity. Variations (or lack thereof) in the bacterioplankton community cannot be explained solely by the distribution of nutrients. For example, the OTU samples in especially $H3_{csub}$ separated along a second PCoA or NMDS axis (Fig. 6a, c), whereas there was much less separation between the nutrient samples (Fig. 6d, f). In contrast, the beta diversity along NMDS1 in nutrient content among the $H1_{surf}$ and $H2_{cmax}$ horizons (Fig. 6f) was markedly greater than the variation in OTU diversity (Fig. 6c). Nutrient distribution in the surface waters did not co-vary with bacterioplankton diversity, but with bacterial abundance, depth, and chl-*a* (Fig. 6f).

Discussion

These results provide some insight into how phytoplankton blooms within the surface waters of the ASP structure heterotrophic bacterioplankton communities throughout the water column. The effects are not confined to the surface waters in which phytoplankton and bacterioplankton co-occur, but also continue below the phytoplankton biomass, with more diverse bacterioplankton communities appearing beneath more abundant phytoplankton blooms. One mechanism responsible for this effect may be that the local impact of the phytoplankton cascades downward as detritus particles from the bloom sink into mesopelagic bacterioplankton communities. At greater depths, the cascading effect diminishes as the particle flux declines with remineralization. In contrast to other recent studies (Galand et al. 2010, Agogué et al. 2011, Alonso-Sáez et al. 2011, Hamdan et al. 2013), hydrologic boundaries (water mass identity) were not the best explanation for bacterial community composition. As an example, the lower WW depth horizon ($H4_{Tmin}$) contained a bacterioplankton community more similar to that of the adjacent and subtending mCDW depth horizon ($H5_{Tmax}$) than to that of the adjacent and overlying upper WW depth horizon ($H3_{csub}$; Fig. 6c).

Mechanisms structuring bacterioplankton communities in surface waters

A distinct subset of bacteria was found in the surface waters, dissimilar and less diverse than

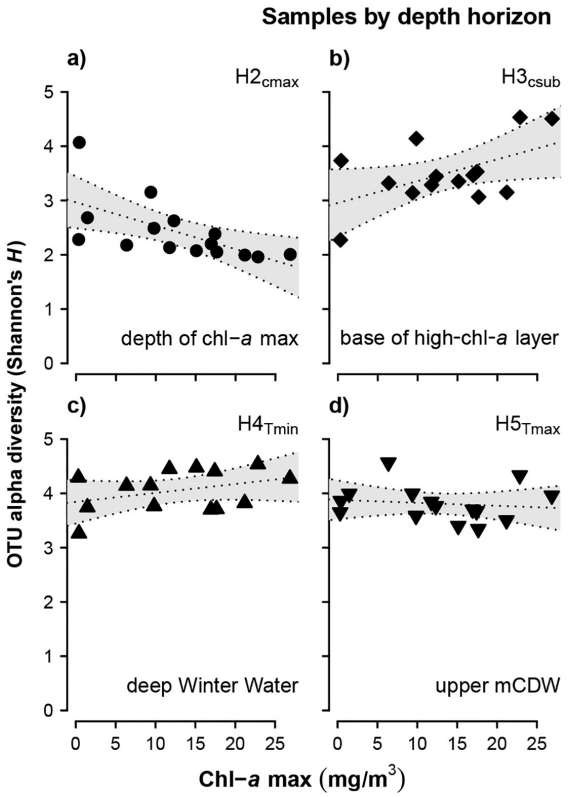

Fig. 5. Relationship between bloom progression as measured by the magnitude of the chl-*a* max at the sampling site and the alpha diversity of OTUs, as measured by Shannon's *H* at four depth horizons: (a) $H2_{cmax}$, the depth of chl-*a* max; (b) $H3_{csub}$, the base of the high-chlorophyll *a* layer; (c) $H4_{Tmin}$, deep Winter Water; and (d) $H5_{Tmax}$, mCDW. Dotted lines represent linear regression results with shaded 95% confidence range.

the underlying mesopelagic community. When local chl-*a* increased, a decrease in bacterioplankton community diversity occurred (Figs. 3a, 5a) along with a decrease in site-to-site community divergence (Fig. 4), all while bacterioplankton abundance increased (Fig. 3b). These results are consistent with the findings of Hyun et al. (2015), who identified a positive correlation between chl-*a* concentration and respiration rates in the open polynya, and with Williams et al. (2016) who reported high bacterial production and increasing exoenzyme activity associated with the bloom. All these patterns may be explained by increasing competition as chl-*a* increases. Bacterioplankton communities in surface waters are structured by local competitive effects that favor specializations for effective heterotrophy in the midst of a highly active phytoplankton community, favoring fast-growing copiotrophs that outcompete slow-growing oligotrophic bacteria. These results are consistent with other community structure data from the region (Delmont et al. 2014, 2015, Kim et al. 2014, Richert et al. 2015, Dinasquet et al. 2017).

These productivity-driven patterns in bacterioplankton community diversity and taxonomic composition in surface waters also agree with the findings of Horner-Devine et al. (2003, 2004), who recognized taxon-specific interactions between productivity and bacterial richness, inferring that copiotrophs profit from high productivity rates and resource availability while putative oligotrophic and more fastidious microbes decrease in abundance with increasing chl-*a*. Direct competition for nutrients with phytoplankton is likely another contributing factor, as phytoplankton can be superior competitors vs. bacterioplankton under high nutrient availability with the opposite seen for more nutrient-poor environments (Kirchman 1994, Løvdal et al. 2007, 2008).

*Cascading effects of chl-*a *with depth*

Bacterioplankton alpha diversity at the $H3_{csub}$ (base of the high-chlorophyll layer) increases as chl-*a* in the overlying surface waters increases (Fig. 5b), showing that the immediate influence of the bloom extends well below its occurrence and that its effect on bacterioplankton community diversity is opposite to that seen in the surface waters. Underneath the euphotic zone, downward flux of diagenetically fresh and labile organic matter fuels heterotrophs (Jiao et al. 2010) and offers a variety of niches. Within the ASP, Delmont et al. (2014) differentiated taxa into characteristic size classes such as particle-associated bacteria which form biofilms or may excrete exoenzymes (e.g., *Colwellia*, *Pseudoalteromonas*, and *Cryomorphaceae*) and free-living bacteria that may scavenge small organic degradation by-products (e.g., *Piscirickettsiaceae*, *Pelagibacter*, *Oceanospirillales*). Our results indicate that broad diversity shifts across photic, carbon, and nutrient gradients accompany this taxonomic turnover, and we expect that similar shifts would occur in similar oceanic systems regardless of the participating taxa.

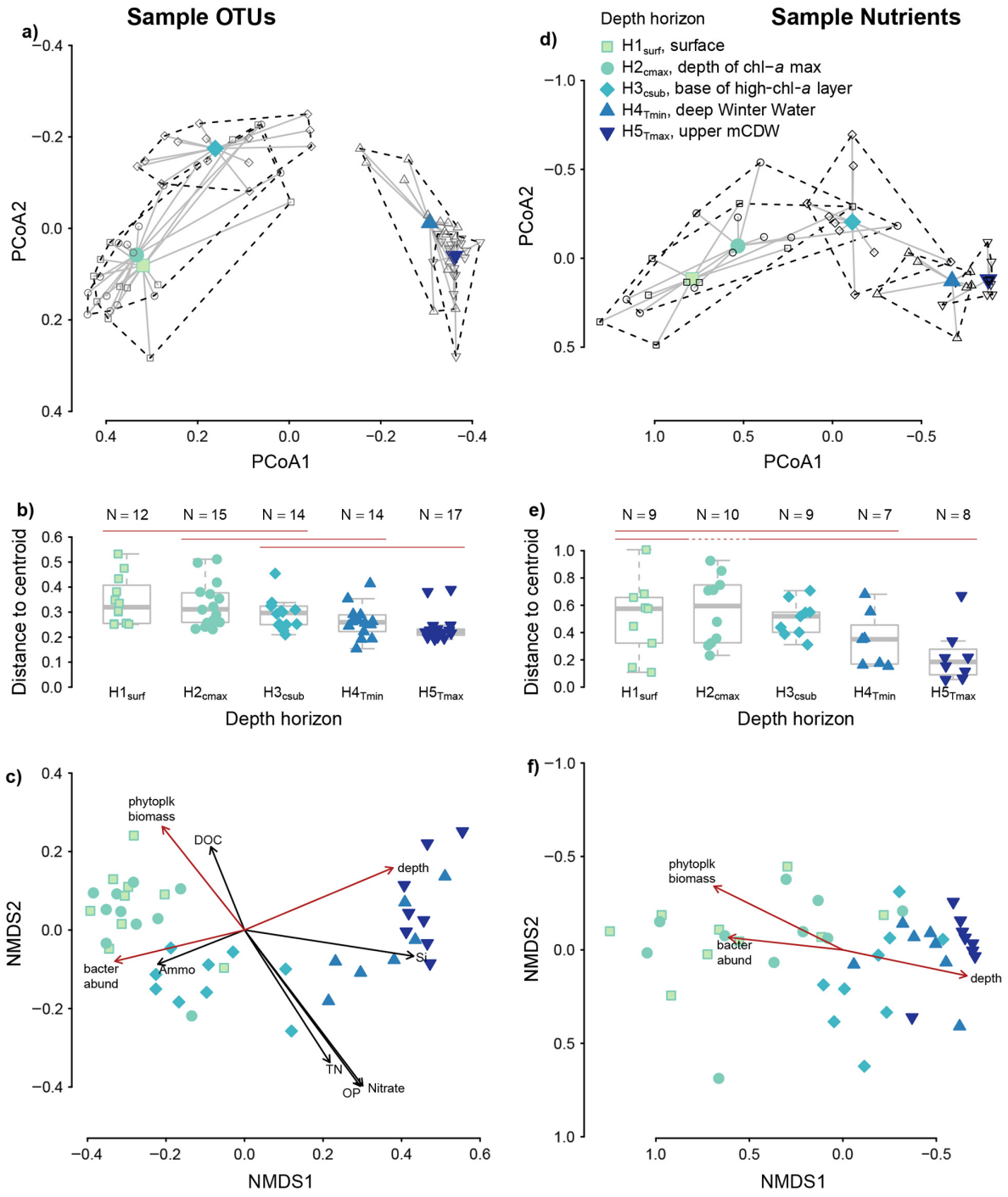

Fig. 6. Multivariate analyses of bacterioplankton community composition and seawater nutrient composition for 43 samples with both OTU (left column) and nutrient data (right column); see text for further details on samples and calculation of pairwise dissimilarities. Panels (a) and (d): the first two axes of principal components analysis (PCoA) with samples grouped by depth horizon (see text for depth horizon definitions). The depth horizon-specific centroid (calculated as the spatial median) is shown as a solid colored symbol following the legend in panel (d). Gray lines connect each centroid to sample-specific values for that depth horizon, and dashed lines

(Fig. 6. *Continued*)
delineate the convex hull surrounding the samples for each depth horizon. Panels (b) and (e): depth horizon-specific distances of samples from the centroid in panels (a) and (d), respectively, as a measure of beta diversity of OTUs and nutrient values within each depth horizon. Solid horizontal lines connect depth horizons that did not differ in beta dispersion, as determined via pairwise Tukey post hoc tests ($P \leq 0.05$); see text for further details. In panel (e), the dashed line segment indicates that $H2_{cmax}$ differed from $H5_{Tmax}$, but $H1_{surf}$ did not. Panels (c) and (f): the first two axes of non-metric multidimensional scaling (NMDS) ordination with samples grouped by depth horizon. Overlying the OTU and nutrient ordinations are corresponding gradients of nutrient composition (panel c) and phytoplankton biomass, bacterioplankton abundance, and sample depth (panels c and f).

As we descend further into the WW, further community and nutrient gradient shifts appear. The lower WW ($H4_{Tmin}$) hosts a bacterioplankton community dissimilar to that found in the upper WW ($H3_{csub}$), and the shift in bacterioplankton community composition revealed by NMDS analysis is pronounced. This is also shown by our bacterioplankton community beta diversity results. Winter water and surface water have similar high beta diversities among samples (Fig. 6a, b), but this similarity appears to mask fundamentally different mechanisms producing this taxonomic turnover. Beta diversity among surface waters is elevated primarily by lateral site-to-site differences in community composition within surface waters and the subtending WW from which populations in these surface communities are recruited each year (Fig. 4), while beta diversity among WW ($H3_{csub}$ and $H4_{Tmin}$) samples is also high because of community differences between samples collected at different depths along the strong gradient of WW bacterioplankton community composition (Fig. 6a–c).

Most nutrients do not show similarly strong gradients within WW ($H3_{csub}$ and $H4_{Tmin}$), with homogenous nutrient composition among deeper samples (Fig. 6f). Silicate, nitrate, and orthophosphate increased gradually with depth, indicating growth-related depletion in the euphotic surface, possibly combined with a downward flux linked to particle sedimentation (Appendix S2: Table S5; Pondaven et al. 2000, Pollard et al. 2006, Paytan and McLaughlin 2007, Yager et al. 2016). In contrast, the highest ammonia and DOC concentrations appear in $H3_{csub}$, where non-migrating macrozooplankton were most abundant (Wilson et al. 2015), while depleted to below detection limits in $H4_{Tmin}$. This may explain some of the variability in bacterioplankton communities of the WW, as ammonia is the most bioavailable form of nitrogen in these waters (Zehr and Ward 2002).

Impact of bacterial community structure on marine carbon sequestration

Mesopelagic bacteria and their organic matter degrading activities are critically important to the fate of sinking photosynthetically derived organic carbon (Azam 1998, Bell et al. 2005). The composition and capabilities of the bacterioplankton community in the mesopelagic WW of the ASP may directly influence the carbon sequestration potential of the phytoplankton bloom occurring in the overlying surface waters (e.g., Mu et al. 2014, Yager et al. 2016). On the basis of these results, it may be inferred that the major nutrient gradient underlying the cascading effects is a change in the quality of particulate organic matter (POM) and dissolved organic matter (DOM) in a continuum with depth from labile to recalcitrant as they cascade downward, and that this explains the shift in bacterioplankton communities from below surface water into the underlying mesopelagic deeper waters. Below the zone of recycling, gradual degradation of POM and DOM transits downward and causes an increased recalcitrance of POM and DOM that is accordingly more likely to undergo long-term storage than microbial recycling. Deeper water masses are known to receive such high C:N and C:P recalcitrant organic carbon (RDOM) formed by microbial modification of labile phytoplankton-derived DOM sources (Jiao et al. 2010).

This sinking phytodetritus provides a source of substrate for organisms at depth, and the cycles arising from this process have been collectively termed the biological carbon pump (Ducklow et al. 2001). One general trend in ocean carbon pump efficiency is that high-latitude regions have higher export efficiency (lower

carbon recycling) than low-latitude regions (Ducklow et al. 2001). Nevertheless, the highly responsive and diverse mesopelagic microbial community we observed is consistent with measurements in Antarctic polynyas showing that most phytodetrital carbon produced during bloom events, representing ~85% of the yearly primary productivity, is recycled within the upper 350 m of the water column (Fischer et al. 1988, Ducklow et al. 2008, 2015).

Conclusion

The massive, recurring phytoplankton bloom in the Amundsen Sea Polynya clearly impacts both the epipelagic and the mesopelagic bacterial community in this key region of the Southern Ocean. The increasing homogeneity of bacterial communities as the algal bloom progresses appears to favor opportunistic heterotrophic taxa, leading to a less diverse bacterial community in the surface waters. In contrast, the bacterial communities in the mesopelagic waters just beneath the bloom become increasingly diverse as the phytoplankton build up and then sink into the subsurface. This sinking phytodetritus provides food for zooplankton and substrate for particle-associated bacteria, which in turn increase the number of biogeochemical niches available at these depths. As the particle remnants sink deeper, their impact on niche availability and bacterial diversity declines, with an increased recalcitrance of POM and DOM that is accordingly more likely to undergo long-term storage than microbial recycling.

As part of ASPIRE, this study provides additional insight to an ecosystem which is undergoing massive changes due to a changing climate. The novelty presented here is the mechanistic view on phytoplankton and bacterioplankton interaction in a polar environment characterized by strong seasonal re-occurring bloom events. Bacterioplankton as decomposers represent the major link between marine primary production from atmospheric carbon and its sequestration into the interior of the ocean.

Acknowledgments

We are grateful to the captain and crew of the Research Icebreaker *Nathanial B. Palmer* and the ASPIRE team supporting us during the cruise, and to the Swedish Polar Research secretariat and Raytheon Polar Services who provided logistic support. The study was funded by the Swedish Research Council (grants to SB and LR) and the U.S. National Science Foundation through the ASPIRE project (ANT-0839069). The 454 pyrosequencing was done at SciLife-Lab SNP/SEQ facility hosted by Uppsala University, and some of our bioinformatic computations were performed at the Uppsala Multidisciplinary Center for Advanced Computational Science (UPPMAX). We thank Alexander Eiler for assistance with handling of the raw pyrosequencing data; Shona Wharton, who produced the GIS map; and Sharon Stammerjohn for help with understanding the ocean water masses.

Literature Cited

Agogué, H., D. Lamy, P. R. Neal, M. L. Sogin, and G. J. Herndl. 2011. Water mass-specificity of bacterial communities in the North Atlantic revealed by massively parallel sequencing. Molecular Ecology 20:258–274.

Alderkamp, A.-C., et al. 2012. Iron from melting glaciers fuels phytoplankton blooms in the Amundsen Sea (Southern Ocean): phytoplankton characteristics and productivity. Deep Sea Research Part II: Topical Studies in Oceanography 71–76:32–48.

Alderkamp, A.-C., et al. 2015. Fe availability drives phytoplankton photosynthesis rates in the Amundsen Sea Polynya. Antarctica. Elementa: Science of the Anthropocene 3:000043.

Alonso-Sáez, L., A. Andersson, F. Heinrich, and S. Bertilsson. 2011. High archaeal diversity in Antarctic circumpolar deep waters. Environmental Microbiology Reports 3:689–697.

Anderson, M. J. 2006. Distance-based tests for homogeneity of multivariate dispersions. Biometrics 62:245–253.

Anderson, M. J., K. E. Ellingsen, and B. H. McArdle. 2006. Multivariate dispersion as a measure of beta diversity. Ecology Letters 9:683–693.

Arrigo, K., and G. van Dijken. 2003. Phytoplankton dynamics within 37 Antarctic coastal polynya systems. Journal of Geophysical Research 108:3271.

Azam, F. 1998. Microbial control of oceanic carbon flux: The plot thickens. Science 280:694–696.

Azam, F., and F. Malfatti. 2007. Microbial structuring of marine ecosystems. Nature Reviews Microbiology 5:782–791.

Barbeau, K., E. L. Rue, K. W. Bruland, and A. Butler. 2001. Photochemical cycling of iron in the surface ocean mediated by microbial iron(III)-binding ligands. Nature 413:409–413.

Bell, T., J. A. Newman, B. W. Silverman, S. L. Turner, and A. K. Lilley. 2005. The contribution of species

richness and composition to bacterial services. Nature 436:1157–1160.

Boström, K., K. Simu, Å. Hagström, and L. Riemann. 2004. Optimization of DNA extraction for quantitative marine bacterioplankton community analysis. Limnology and Oceanography: Methods 2:365–373.

Bray, J. R., and J. T. Curtis. 1957. An ordination of the upland forest communities of Southern Wisconsin. Ecological Monographs 27:326–349.

Bryant, D. A., and N.-U. Frigaard. 2006. Prokaryotic photosynthesis and phototrophy illuminated. Trends in Microbiology 14:488–496.

Buesseler, K. O., and P. W. Boyd. 2009. Shedding light on processes that control particle export and flux attenuation in the twilight zone of the open ocean. Limnology and Oceanography 54:1210–1232.

Buesseler, K. O., et al. 2007. Revisiting carbon flux through the ocean's Twilight Zone. Science 316:567–570.

Caporaso, J., et al. 2010. QIIME allows analysis of high-throughput community sequencing data. Nature Methods 7:335–336.

Colwell, R. K., A. Chao, N. J. Gotelli, S. Y. Lin, C. X. Mao, R. L. Chazdon, and J. T. Longino. 2012. Models and estimators linking individual-based and sample-based rarefaction, extrapolation and comparison of assemblages. Journal of Plant Ecology 5:3–21.

Delmont, T. O., A. M. Eren, J. H. Vineis, and A. F. Post. 2015. Genome reconstructions indicate the partitioning of ecological functions inside a phytoplankton bloom in the Amundsen Sea, Antarctica. Frontiers in Microbiology 6:1090.

Delmont, T. O., K. M. Hammar, H. W. Ducklow, P. L. Yager, and A. F. Post. 2014. Bacterial community structure in the Amundsen Sea Polynya is shaped by *Phaeocystis antarctica* blooms. Systems Microbiology 5:646.

Dinasquet, J., I. Richert, R. Logares, P. L. Yager, S. Bertilsson, and L. Riemann. 2017. Mixing of water masses caused by a drifting iceberg affects bacterial activity, community composition and substrate utilization capability in the Southern Ocean. Environmental Microbiology 19:2453–2467.

Ducklow, H. W., M. Erickson, J. Kelly, M. Montes-Hugo, C. A. Ribic, R. C. Smith, S. E. Stammerjohn, and D. M. Karl. 2008. Particle export from the upper ocean over the continental shelf of the west Antarctic Peninsula: a long-term record, 1992–2007. Deep Sea Research Part II: Topical Studies in Oceanography 55:2118–2131.

Ducklow, H., D. Steinberg, and K. Buesseler. 2001. Upper ocean carbon export and the biological pump. Oceanography 14:50–58.

Ducklow, H. W., S. E. Wilson, A. F. Post, S. E. Stammerjohn, M. Erickson, S. Lee, K. E. Lowry, R. M. Sherrell, and P. L. Yager. 2015. Particle flux on the continental shelf in the Amundsen Sea Polynya and Western Antarctic Peninsula. Elementa: Science of the Anthropocene 3:000046.

Ducklow, H., and P. L. Yager. 2007. Pelagic bacteria in polynyas. Pages 323–361 *in* W. O. Smith and D. Barber, editors. Polynyas: windows into Polar Oceans. Elsevier, Amsterdam, The Netherlands.

Edgar, R. 2010. Search and clustering orders of magnitude faster than BLAST. Bioinformatics 26:2460–2461.

Fischer, G., D. Fütterer, R. Gersonde, S. Honjo, D. Ostermann, and G. Wefer. 1988. Seasonal variability of particle flux in the Weddell Sea and its relation to ice cover. Nature 335:426–428.

Galand, P. E., M. Potvin, E. O. Casamayor, and C. Lovejoy. 2010. Hydrography shapes bacterial biogeography of the deep Arctic Ocean. ISME Journal 4:564–576.

Gasol, J., and P. del Giorgio. 2000. Using flow cytometry for counting natural planktonic bacteria and understanding the structure of planktonic bacterial communities. Scientia Marina 64:197–224.

Ghiglione, J. F., et al. 2012. Pole-to-pole biogeography of surface and deep marine bacterial communities. Proceedings of the National Academy of Sciences of USA 109:17633–17638.

Giering, S. L. C., et al. 2014. Reconciliation of the carbon budget in the ocean's twilight zone. Nature 507:480–483.

Gómez-Consarnau, L., J. M. González, M. Coll-Lladó, P. Gourdon, T. Pascher, R. Neutze, C. Pedrós-Alió, and J. Pinhassi. 2007. Light stimulates growth of proteorhodopsin-containing marine Flavobacteria. Nature 445:210–213.

Hamdan, L. J., R. B. Coffin, M. Sikaroodi, J. Greinert, T. Treude, and P. M. Gillevet. 2013. Ocean currents shape the microbiome of Arctic marine sediments. ISME Journal 7:685–696.

Haran, T., J. Bohlander, T. Scambos, T. Painter, and M. Fahnestock. 2005. Compilers. MODIS Mosaic of Antarctica (MOA) Image Map. National Snow and Ice Data Center. National Snow and Ice Data Center, Boulder, Colorado, USA.

Herlemann, D., M. Labrenz, K. Jürgens, S. Bertilsson, J. Waniek, and A. Andersson. 2011. Transitions in bacterial communities along the 2000 km salinity gradient of the Baltic.

Horner-Devine, M. C., K. M. Carney, and B. J. M. Bohannan. 2004. An ecological perspective on bacterial biodiversity. Proceedings of the Royal Society of London B 271:113–122.

Horner-Devine, M. C., M. A. Leibold, V. H. Smith, and B. J. M. Bohannan. 2003. Bacterial diversity patterns along a gradient of primary productivity. Ecology Letters 6:613–622.

Hyun, J.-H., S.-H. Kim, E. J. Yang, A. Choi, and S. H. Lee. 2015. Biomass, production, and control of heterotrophic bacterioplankton during a late phytoplankton bloom in the Amundsen Sea Polynya, Antarctica. Deep Sea Research Part II: Topical Studies in Oceanography. https://doi.org/10.1016/j.dsr2.2015.10.001

Jiao, N., et al. 2010. Microbial production of recalcitrant dissolved organic matter: long-term carbon storage in the global ocean. Nature Reviews Microbiology 8:593–599.

Kim, J.-G., et al. 2014. Unveiling abundance and distribution of planktonic Bacteria and Archaea in a polynya in Amundsen Sea, Antarctica. Environmental Microbiology 16:1566–1578.

Kiørboe, T., and G. A. Jackson. 2001. Marine snow, organic solute plumes, and optimal chemosensory behavior of bacteria. Limnology and Oceanography 46:1309–1318.

Kirchman, D. L. 1994. The uptake of inorganic nutrients by heterotrophic bacteria. Microbial Ecology 28:255–271.

Lauro, F. M., et al. 2009. The genomic basis of trophic strategy in marine bacteria. Proceedings of the National Academy of Sciences of USA 106:15527–15533.

Legendre, P., and H. J. B. Birks. 2012. From classical to canonical ordination. Pages 201–248 *in* H. J. B. Birks, A. F. Lotter, S. Juggins, and J. P. Smol, editors. Tracking Environmental Change Using Lake Sediments: data Handling and Numerical Techniques. Developments in Paleoenvironmental Research, vol. 5. Springer, Dordrecht, The Netherlands.

Longhurst, A. R., and W. Glen Harrison. 1989. The biological pump: profiles of plankton production and consumption in the upper ocean. Progress in Oceanography 22:47–123.

Løvdal, T., C. Eichner, H.-P. Grossart, V. Carbonnel, L. Chou, and T. F. Thingstad. 2008. Competition for inorganic and organic forms of nitrogen and phosphorous between phytoplankton and bacteria during an *Emiliania huxleyi* spring bloom (PeECE II). Biogeosciences Discussions 4:3343–3375.

Løvdal, T., T. Tanaka, and T. F. Thingstad. 2007. Algal-bacterial competition for phosphorus from dissolved DNA, ATP, and orthophosphate in a mesocosm experiment. Limnology and Oceanography 52:1407–1419.

Mu, L., S. E. Stammerjohn, K. E. Lowry, and P. L. Yager. 2014. Spatial variability of surface *p*CO2 and air-sea CO2 flux in the Amundsen Sea Polynya. Antarctica. Elementa: Science of the Anthropocene 3:000036.

Oksanen, J., F. G. Blanchet, R. Kindt, P. Legendre, P. R. Minchin, R. B. O'Hara, G. L. Simpson, P. Solymos, M. H. H. Stevens, and H. Wagner. 2013. vegan: community Ecology Package. R package version 2.3-1. https://CRAN.R-project.org/package=vegan

Paytan, A., and K. McLaughlin. 2007. The oceanic phosphorus cycle. Chemical Reviews 107:563–576.

Pelve, E. A., K. M. Fontanez, and E. F. DeLong. 2017. Bacterial Succession on Sinking Particles in the Ocean's Interior. Frontiers in Microbiology 8:2269.

Pollard, R., P. Tréguer, and J. Read. 2006. Quantifying nutrient supply to the Southern Ocean. Journal of Geophysical Research: Oceans 111:C05011.

Pondaven, P., O. Ragueneau, P. Tréguer, A. Hauvespre, L. Dezileau, and J. L. Reyss. 2000. Resolving the "opal paradox" in the Southern Ocean. Nature 405:168–172.

Quast, C., E. Pruesse, P. Yilmaz, J. Gerken, T. Schweer, P. Yarza, J. Peplies, and F. Glockner. 2013. The SILVA ribosomal RNA gene database project: improved data processing and web-based tools. Nucleic Acids Research 41:D590–D596.

Quince, C., A. Lanzen, R. J. Davenport, and P. J. Turnbaugh. 2011. Removing noise from pyrosequenced amplicons. BMC Bioinformatics 12:38.

Ramette, A. 2007. Multivariate analyses in microbial ecology. FEMS Microbiology Ecology 62:142–160.

Randall-Goodwin, E., et al. 2015. Freshwater distributions and water mass structure in the Amundsen Sea Polynya region, Antarctica. Elementa: Science of the Anthropocene 3:000065.

Reid, R. T., D. H. Livet, D. J. Faulkner, and A. Butler. 1993. A siderophore from a marine bacterium with an exceptional ferric ion affinity constant. Nature 366:455–458.

Richert, I., J. Dinasquet, R. Logares, L. Riemann, P. L. Yager, A. Wendeberg, and S. Bertilsson. 2015. The influence of light and water mass on bacterial population dynamics in the Amundsen Sea Polynya. Elementa: Science of the Anthropocene 3:000044.

Riemann, L., G. Steward, and F. Azam. 2000. Dynamics of bacterial community composition and activity during a mesocosm Diatom bloom. Applied and Environmental Microbiology 66:578–587.

Schofield, O., T. Miles, A.-C. Alderkamp, S.-H. Lee, C. Haskins, E. Roglsky, R. E. Sipler, R. M. Sherrell, and P. L. Yager. 2015. In situ phytoplankton distributions in the Amundsen Sea polynya measured by autonomous gliders. Elementa: Science of the Anthropocene 3:000073.

Scofield, D. G., P. E. Smouse, J. Karubian, and V. L. Sork. 2012. Use of alpha, beta, and gamma

diversity measures to characterize seed dispersal by animals. American Naturalist 180:719–732.

Seymour, J. R., S. A. Amin, J.-B. Raina, and R. Stocker. 2017. Zooming in on the phycosphere: the ecological interface for phytoplankton–bacteria relationships. Nature Microbiology 2:17065.

Shannon, C. E. 1948. A mathematical theory of communication. Bell System Technical Journal 27:379–423.

Simpson, E. H. 1949. Measurement of diversity. Nature 163:688.

Sipler, R. E., and T. L. Connelly. 2015. Bioavailability of surface dissolved organic matter to aphotic bacterial communities in the Amundsen Sea Polynya, Antarctica. Elementa: Science of the Anthropocene 3:000060.

Wang, Q., G. Garrity, J. Tiedje, and J. Cole. 2007. Naïve Bayesian classifier for rapid assignment of rRNA sequences into the new bacterial taxonomy. Applied and Environmental Microbiology 73: 5261–5267.

Williams, C. M., A. M. Dupont, J. Loevenich, A. F. Post, J. Dinasquet, and P. L. Yager. 2016. Pelagic microbial heterotrophy in response to a highly productive bloom of *Phaeocystis antarctica* in the Amundsen Sea Polynya, Antarctica. Elementa: Science of the Anthropocene 4:000102.

Wilson, S. E., R. Swalethrop, S. Kjellerup, M. A. Wolverton, H. W. Ducklow, and P. L. Yager. 2015. Meso- and macro-zooplankton community structure of the Amundsen Sea Polynya, Antarctica (Summer 2010–2011). Elementa: Science of the Anthropocene 3:000033.

Yager, P. L., T. L. Connelly, B. Mortazavi, K. E. Wommack, N. Bano, J. E. Bauer, S. Opsahl, and J. T. Hollibaugh. 2001. Dynamic bacterial and viral response to an algal bloom at sub-zero temperatures. Limnology and Oceanography 46:790–801.

Yager, P. L., et al. 2012. ASPIRE: the Amundsen Sea polynya international research expedition. Oceanography 25:30–43.

Yager, P., et al. 2016. A carbon budget for the Amundsen Sea Polynya, Antarctica: estimating net community production and export in a highly productive polar ecosystem. Elementa: Science of the Anthropocene 4:000140.

Zehr, J. P., and B. B. Ward. 2002. Nitrogen Cycling in the Ocean: new Perspectives on Processes and Paradigms. Applied and Environmental Microbiology 68:1015–1024.

Supporting Information

Additional Supporting Information may be found online at: http://onlinelibrary.wiley.com/doi/10.1002/ecs2.2641/full